Journal of Materials Chemistry C

ROYAL SOCIETY OF CHEMISTRY

PAPER

View Article Online
View Journal

Cite this: DOI: 10.1039/d5tc03779d

The role of the donor in the light-induced degradation of Y6 non-fullerene acceptors in PM6:Y6 blend films

Suraj Prasad, C. Moyses Araujo and Ellen Moons *

Despite the rapid advancements in the performance of organic solar cells (OSCs), improving their operational lifetime remains a significant challenge. The photodegradation of donor polymer PM6, small molecule non-fullerene acceptor (NFA) Y6, and their blend was investigated under ambient conditions. To photodegrade the spin-coated thin films, samples were exposed to AM 1.5 illumination, as well as UV-filtered and long-wavelength-filtered light. The evolution of their properties upon increasing the exposure time up to 45 h was monitored using UV-vis absorption, Fourier transform infrared (FTIR), and photoemission spectroscopy. The results demonstrate that neat PM6 films exhibit faster absorbance loss than the neat Y6 films. This is accompanied by the formation of new carbonyl groups on PM6, while only minor indications of photooxidation were observed in degraded Y6 films. The valence band spectra of Y6 remain unchanged upon photodegradation. Interestingly, the photobleaching rate of Y6 in PM6:Y6 blend films was found to be higher than that of neat Y6 films. XPS spectra of C 1s and S 2p confirm that photooxidation products formed in PM6 and PM6:Y6 films, evidenced by new oxidized carbonyl C 1s and oxidized sulfur S 2p peaks. Under AM 1.5 illumination, several photooxidation pathways can be active, involving the formation of both superoxide radicals and singlet oxygen species and their subsequent oxidation reactions with conjugated molecules. Using filtered light conditions, these different degradation pathways could be separated. Upon exposure to long-wavelength-filtered light, which is predominantly absorbed by the Y6 acceptor, the generation of superoxide radicals is significantly suppressed, resulting in enhanced photostability of the blend compared to illumination with unfiltered light. The remaining photodegradation of the blend components under these illumination conditions can therefore be ascribed to energy transfer from the photosensitizing acceptor, feeding into the singlet oxygen formation. These insights could inspire the design of new donor and acceptor materials with improved photostability by tuning the positions of their singlet and triplet states to minimize the formation of oxygen-mediated reactive species.

Received 21st October 2025,
Accepted 21st December 2025

DOI: 10.1039/d5tc03779d

rsc.li/materials-c

1. Introduction

Organic solar cells (OSCs) are an emerging photovoltaic technology, driven by their unique advantages, such as mechanical flexibility, light weight, the potential for cost-effective large-area fabrication,[1–3] and their short energy payback time.[4–6] Over the past decade, following the synthesis of non-fullerene acceptors (NFAs)[7,8] and the development of various processing strategies for active layers, OSCs have shown a tremendous improvement in power conversion efficiency (PCE), now exceeding 19% for single junction solar cells.[9–11] However, the operational lifetime of OSCs is limited, which remains a challenge for outdoor use.[12–14] To address the limited lifetime, it is essential to understand the degradation mechanisms of OSCs and their molecular constituents, including the effect of environmental factors, such as light, heat, moisture, and oxygen.[15–17] Light, in particular high-energy photons in the UV spectral range, can independently induce photodegradation of molecular materials[18,19] and degrade the OSC's performance.[18] In the presence of oxygen and water vapor that diffuse into the active layer of the devices,[20,21] their exposure to light can lead to photooxidation of not only the donor and acceptor components but also the electrodes and interface layers.[19,22] One of the strategies to avoid this (photo)chemical degradation by air components is to adequately encapsulate the OSCs.[23–25] Heat is another degradation factor that can contribute to changes in the morphology.[26]

It has been established that two types of oxygen-mediated species may contribute to the degradation of performance in fullerene- and NFA-based OSCs: superoxide radicals (O_2^-) and

Department of Engineering and Physics, Karlstad University, SE-65188 Karlstad, Sweden. E-mail: ellen.moons@kau.se

the reactive singlet oxygen ($^1O_2$) species.[27–29] A superoxide anion can be generated through photoinduced electron transfer from an excited molecular state to a dioxygen molecule in the environment, provided that the excited state has a higher energy than the reduction potential of O_2.[29,30] In contrast, the $^1O_2$ species is formed by energy transfer from the triplet excited state of a molecule (photo-sensitizer) to ground state molecular oxygen. Upon photoexcitation of the blend, one of the components, either the donor or the acceptor, or both, can trigger photochemical reactions, forming oxygen-based radical species, such as hydroxyl and alkylperoxyl radicals, which can further drive the photooxidation of the donor or acceptor.[27] All these factors can significantly impact the stability and lifetime of unencapsulated OSCs under ambient conditions. While encapsulated devices demonstrate substantially longer operational lifetimes, the diffusion of air components through non-ideal encapsulants, particularly through sealants and flexible substrates, remains a significant degradation pathway. To improve the photostability of the active layers/devices, various strategies have been applied, for example, materials design,[23,31] solvent additives,[32] and UV absorbents.[33–35] We and others have previously demonstrated that, relative to fullerene acceptors, most NFAs exhibit superior photostability under ambient air conditions.[19,36,37] In our previous work, we elucidated the influence of the molecular structure, in particular, the presence of the BDT moiety, on photodegradation by comparing three NFAs: Y5, PYT, and PF5-Y5.[19] The results demonstrate that replacing the BDT moiety in PF5-Y5 with a thiophene unit in PYT significantly improved the acceptor polymer's intrinsic photostability under AM 1.5 illumination in air. Films of the small molecule acceptor Y5 are also significantly more resistant to photooxidation than the BDT-containing Y5-based copolymer PF5–Y5. Here, we demonstrate that blending the Y-type NFA Y6 with the polymer donor PM6 leads to an accelerated photodegradation of Y6. Wang *et al.* studied the photodegradation of Y6, blended with three different donor polymers, PTQ10, PM6, and D18, under white light in air.[38] The authors concluded from *in situ* Raman spectroscopy that the twisting of the BDT moiety in PM6 and D18 was the major cause of the photodegradation. In contrast, PTQ10, which does not contain a BDT moiety, exhibited better photostability.[38,39] In a photodegradation study of PM6:Y6 blend films in a N_2 atmosphere, Liu *et al.* demonstrated that the photochemical decomposition of Y6 by UV photons is responsible for the degradation of the PM6:Y6 solar cells.[40] The authors concluded from matrix-assisted laser desorption ionization time-of-flight (MALDI-TOF) mass spectrometry that the breaking of the linkage bond between the core and end groups of Y6 was responsible for the photodegradation.[40]

This study aims to elucidate the contributions of the individual components in PM6:Y6 blend films. UV-vis spectra show that the absorbance of neat Y6 films is relatively stable under exposure to AM 1.5 illumination in air, compared to that of neat PM6 films. We also found that in PM6:Y6 blend films, the acceptor Y6 undergoes photodegradation at a faster rate than in neat Y6 films. To understand the contributions of the donor and acceptor to the light-induced degradation of the PM6:Y6 blend film, we investigated their wavelength-dependent photodegradation by exposing the samples to filtered AM 1.5 light using 400 nm (LP400) and 665 nm (LP665) long-pass filters. The degradation rates of both donor and acceptor components in the PM6:Y6 blend films were observed to decrease under LP400 and LP665 illumination, consistent with the reduced light intensity. Nevertheless, even after compensating for the decrease in illuminance, the blend films exhibited slower bleaching and formed fewer photooxidation products under LP665 illumination. This is because the donor does not significantly absorb high-wavelength light, and therefore, the formation of superoxide is hindered under these conditions. This suggests that the remaining photodegradation of the donor and acceptor under LP665 illumination is likely due to singlet oxygen formation *via* energy transfer from the photosensitizing acceptor. IR spectra of pure PM6 and PM6:Y6 blend films confirm the formation of new carbonyl groups and breaking of the original quinone group, whereas in pure Y6 films, no significant changes were observed, a finding further corroborated by C 1s and S 2p core-level XPS spectra. The results of this study unravel the photooxidation pathways in PM6:Y6 blends under illumination and ambient conditions and provide insights into the importance of the energy levels of the donor and acceptor when aiming at materials for OSCs with enhanced photostability.

2. Experimental

2.1 Materials and sample preparation

The donor polymer PM6 was purchased from 1-Material Inc. and the acceptor Y6 was purchased from Sigma Aldrich, respectively. The molecular weight (M_w) of Y6 is 1451.93 g mol^{-1}, and for PM6, it is 120 000 g mol^{-1} with PDI $\sim$ 2.5, respectively. Chloroform was purchased from Sigma Aldrich (anhydrous, 99.8%). Thin films were deposited on glass substrates for UV-vis absorption spectroscopy and atomic force microscopy (AFM), on KBr pellets for FTIR spectroscopy, and on silicon substrates for photoelectron spectroscopy. The glass substrates were cleaned with acetone and 2-propanol for 10 min each, in an ultrasonic bath, and then UV-ozone treated for 10 min. The KBr substrates (diameter 13 mm, Thermo Fisher Scientific, USA) were used as is. The n-type SiO_x/Si (001) substrates were cleaned using a standard RCA procedure, omitting the final hydrofluoric acid etching step. The coating solutions with a concentration of 16 mg mL^{-1} in chloroform were stirred overnight at room temperature. Thin films were spin-coated inside a N_2 filled glove box (O_2 < 10 ppm, H_2O < 0.1 ppm) (MB200MOD, MBraun Inertgas-Systeme GmbH, Germany) at 3000 rpm for 60 seconds (except for PM6 coated at 6000 rpm for 60 s) and annealed immediately at 100 °C for 10 min. The thin films were degraded by exposing them in air to white light (AM 1.5) from the solar simulator Sol2A (model 94022A, Oriel Instruments) without filter and with long-pass filters λ > 400 nm (LP400) and λ > 665 nm (LP665) placed between the lamp and the sample. By using the LP400 and LP665 filters, the light intensity is reduced from 1000 W m^{-2} to $\sim$926 W m^{-2} and $\sim$607 W m^{-2}, respectively.

The exposure was done stepwise on the same sample for the chosen exposure times of 30 min, 2 h, 10 h, 24 h, and 45 h.

2.2 Experimental methods

The UV-vis absorption spectra were collected in transmission mode between 300 and 1000 nm with a Cary 5000 UV-vis-NIR spectrophotometer (Agilent Technologies, USA), equipped with Cary WinUV 6.1 software. For the background measurements, a cleaned glass substrate was used as a reference sample, and its spectrum was subtracted from the measured spectrum of the thin film coated on glass. Fourier transform infrared (FTIR) spectra of the thin films on KBr platelets were recorded in transmission mode in the wavenumber range of 600–4000 cm^{-1} using an INVENIO S spectrometer (Bruker, France) purged with dry air and equipped with OPUS 8.5 software. The sample thickness and morphology were determined using a Nanoscope 8 Multimode AFM (Bruker, France) in tapping mode with AFM tips (RTESPA-300) purchased from Bruker. The thickness of the films was determined by scanning the AFM tip across a scratch made in the film. The film thicknesses for PM6, Y6, and PM6:Y6 were 94 nm, 72 nm, and 94 nm, respectively. The high-resolution X-ray photoelectron spectroscopy (XPS) measurements were carried out at the FlexPES beamline of the MAX IV synchrotron in Lund, Sweden.[41] The experiments used a defocused X-ray beam with a slit size of 5 μm and a Scienta DA-30L (W) electron analyzer, operated at normal emission, with a pass energy of 50 eV. For the XPS measurements, the different core levels were measured at the same kinetic energy of approximately 60 eV to maintain a consistent information depth. The photon energies used for the F 1s, O 1s, N 1s, C 1s, and S 2p core levels were 750 eV, 590 eV, 465 eV, 350 eV, and 225 eV, respectively. For the VB spectrum and secondary electron cutoff (SECO) measurements, a photon energy of 45 eV was used, and a negative bias of 28.46 V was applied to the sample holder. The system was maintained at an ultra-high vacuum with a base pressure of 3×10^{-10} mbar. The core level spectra were fitted using CasaXPS software,[42] applying a composite peak shape, consisting of 30% Lorentzian and 70% Gaussian components. The sulfur 2p doublet ($2p_{3/2}$ and $2p_{1/2}$) was fitted with a fixed energy separation of 1.18 eV, a consistent 2 : 1 intensity ratio, and equal full widths at half maximum (FWHM).[43] For quantitative analysis, a Shirley background subtraction method was utilized.[44,45]

3. Results and discussion

3.1 Photobleaching of pristine and blend films

Fig. 1(a) and (b) show the chemical structures of the donor polymer PM6 and the NFA Y6, respectively. The optical absorption

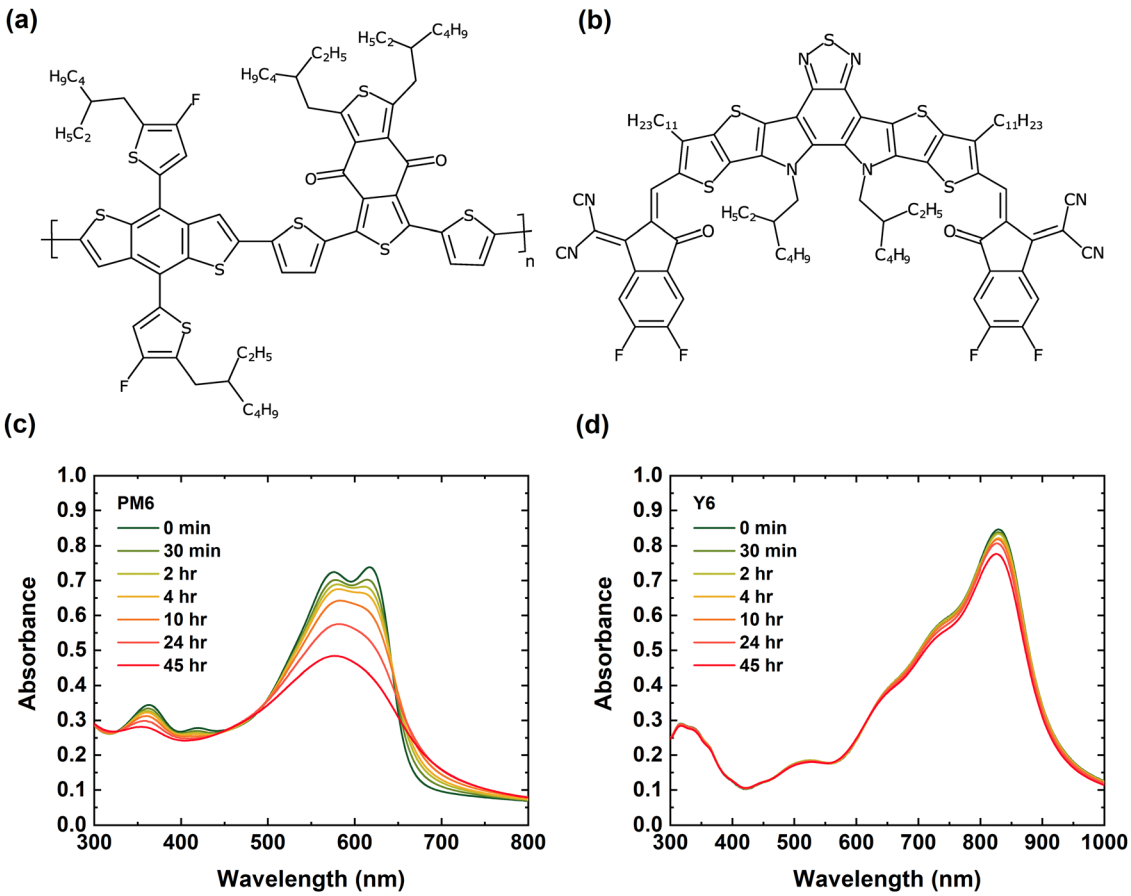

Fig. 1 The chemical structures of (a) PM6 and (b) Y6. The optical absorption spectra of spin-coated films of (c) PM6 and (d) Y6, unexposed and exposed in air under AM 1.5 (unfiltered) light for 30 min, 2 h, 4 h, 10 h, 24 h, and 45 h.

spectra of PM6 and Y6 films are shown in Fig. 1(c) and (d). The main absorption bands of PM6 have maxima at 575 nm and 617 nm, corresponding to the $A_{0\text{-}1}$ and $A_{0\text{-}0}$ transitions, respectively,[46,47] and smaller absorption peaks at 364 nm and 420 nm. The spectrum resembles that of PBDB-T films.[19] Upon illumination to AM 1.5 light in air, the absorbance of the $A_{0\text{-}1}$ and $A_{0\text{-}0}$ peaks decreases, reaching absorbance losses of 33% and 42% after 45 h, respectively, as presented in Table 1. The absorbance of the peaks at 364 nm and 420 nm has decreased by 19% and 12% after 45 h of exposure, while the absorbance increases slightly in the 450–500 nm region with increasing exposure time. Also, an increase in the absorption tail is observed in the range of 700–800 nm, which could indicate the formation of sub-gap energy states upon photodegradation.[19,38] An isosbestic point is located at 649 nm, where the absorbance is independent during the photochemical reaction.

For Y6, the intensity of the main absorption peak at 828 nm decreases by 8% upon exposure to AM 1.5 light in air for 45 h, and the shoulder peak at around 735 nm decreases slightly, while the other absorption bands with maxima at shorter wavelengths (317 nm and 520 nm) remain unaffected. From the UV-vis absorption spectra, it can be concluded that the donor PM6 film photobleaches significantly faster than the acceptor Y6 film. Values for the relative absorbance losses after 45 h of exposure are summarized in Table 1 and the evolution of the normalized absorbance at selected wavelengths, corresponding to the absorption maxima, is summarized in Fig. S1. As a subsequent step, the optical absorption spectra of fresh and photodegraded PM6 : Y6 (1 : 1) blend films were recorded and systematically compared with those of the corresponding pristine neat films of PM6 and Y6.

Fig. 2 shows the absorption spectra of fresh and photodegraded PM6:Y6 blend films. The degraded films were continuously exposed in air to AM 1.5 without a filter, with a 400 nm long-pass filter (LP400), and with a 665 nm long-pass filter (LP665), before measuring their absorption spectra. The transmission spectra of the LP400 and LP665 filters are shown in Fig. S3. In the absorption spectra of the unexposed PM6:Y6 blend film (Fig. 2(a)–(c)), the main absorption peaks are located at 582 nm and 627 nm, primarily from PM6, and at 814 nm, uniquely from Y6. Compared to the pure films, the absorption maxima in the blend film have shifted slightly, to longer wavelengths (by 10 nm) for the 582 and 627 nm peaks (compared to neat PM6) and to shorter wavelengths (by 14 nm) for the 814 nm peak (compared to neat Y6). These shifts may result from donor–acceptor interactions or differences in molecular packing between the blend and neat films.

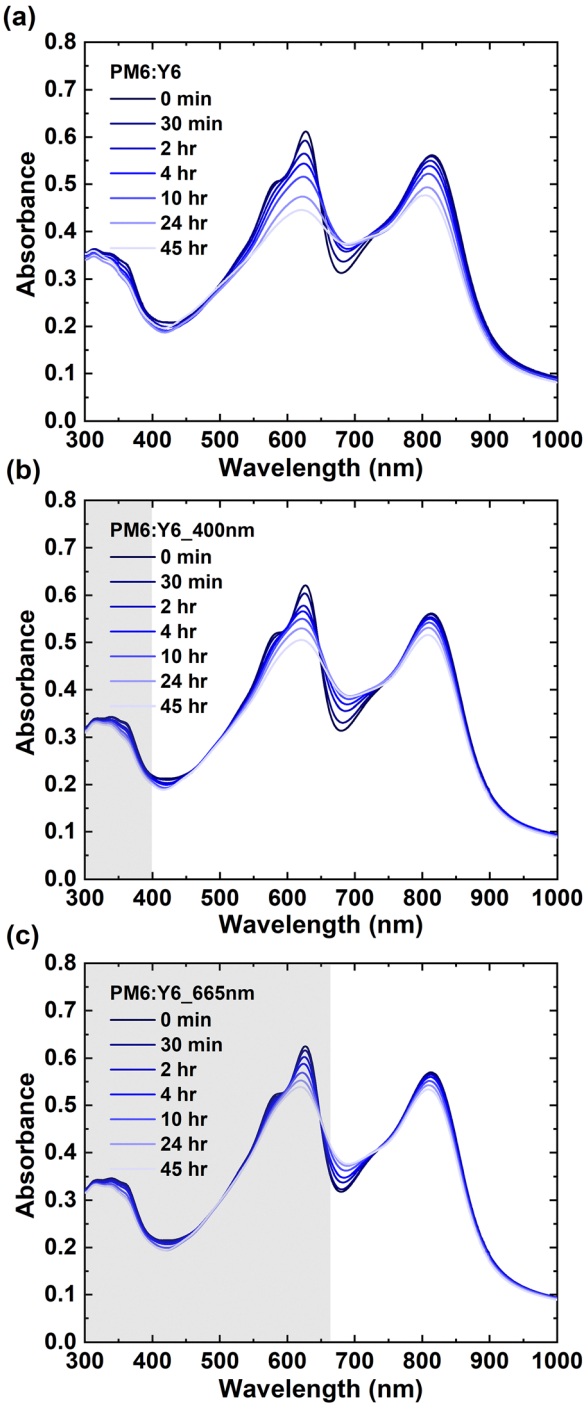

Fig. 2 The optical absorption spectra of spin-coated PM6 : Y6 (1 : 1) films measured in air before and after photodegradation by exposure for different times (30 min, 2 h, 10 h, 24 h, and 45 h) to AM1.5 light in air without filter (a), with LP400 filter (b), and with LP665 filter (c). The grey area indicates the part of the spectrum that is blocked by the filter during the degradation process.

Table 1 The relative change in absorbance of PM6, Y6, and PM6:Y6 blend films at given wavelengths after 45 h of exposure to different illumination conditions, extracted from Fig. 1, 2, and Fig. S2

Filters	PM6 in the neat film (at 617 nm) (%)	PM6 in the blend film (at 627 nm) (%)	Y6 in the neat film (at 828 nm) (%)	Y6 in the blend film (at 814 nm) (%)
No filter	42	27	8	16
LP 400	25	19	4	9
LP 665	6	15	3	7

Upon illumination under AM 1.5 light in air, the absorbance at the wavelengths corresponding to the $A_{0\text{-}0}$ and $A_{0\text{-}1}$ bands of PM6 decreases, reaching an absorbance loss after 45 h of 27%

and 18%, respectively, as presented in Table 1. The absorbance at 814 nm, originating from Y6 in the blend film, was reduced by 16% after 45 h of exposure. Values for the relative absorbance losses after 45 h of exposure are summarized in Table 1 and the evolution of the normalized absorbance at selected wavelengths, corresponding to the absorption maxima, with exposure time, is summarized in Fig. S1. Comparison of the values in Table 1 shows that the degradation of Y6 is accelerated in the PM6:Y6 blend film relative to the neat Y6 film. It is noted that an increase in absorbance is observed in the wavelength range of 658–722 nm for the blend, similar to that observed in the pure PM6 spectra. This increase may indicate the formation of new species during photodegradation.

3.2 Degradation processes in the blend film

The photodegradation of the donor–acceptor blend film in air can be divided into three different mechanisms: (1) the absorption of photons, including high-energy photons by the donor and acceptor; (2) the formation of superoxide radicals (O_2^-) and/or singlet oxygen ($^1O_2$); and (3) the reaction of the reactive oxygen species (ROS) with the conjugated molecules.[30,48–51] All three possible degradation pathways can be active under unfiltered light and LP400 filtered light: (1) direct photodegradation; (2) photooxidation *via* a superoxide anion, formed by electron transfer; and (3) photooxidation by singlet oxygen, formed by energy transfer. If an energy level lies above the reduction potential of O_2 (3.75 eV), as illustrated for the donor in Fig. 3(a), electron transfer from the excited state to molecular oxygen can occur, leading to the formation of a superoxide radical.[29,30] When the excited-state energy of the molecule lies below the reduction potential of O_2, electron transfer to molecular oxygen is hindered, as illustrated in Fig. 3(a) for Y6. In this case, energy transfer from the acceptor triplet state to ground-state triplet oxygen can occur, generating singlet oxygen (Fig. 3(b)).

Fig. 3(a) and (b) illustrate the allowed photophysical processes: electron transfer from the donor LUMO to ground-state oxygen, forming superoxide species, and energy transfer from the acceptor to ground-state oxygen, generating singlet oxygen. Once formed, these reactive species can react with the conjugated molecules PM6 and Y6 in the blend film, resulting in the formation of oxidation products. To investigate the effect of high-energy UV photons, the PM6:Y6 thin film is compared with the one exposed to LP400-filtered light, which excludes UV photons. The absorption spectra of PM6:Y6 films under the LP400 filtered light are shown in Fig. 2(b). The absorbance of PM6 and Y6 components in the PM6:Y6 blend film decreased by 19% and 9%, respectively, after 45 h of LP400 illumination, as shown in Table 1. Compared to pure component films, these absorption losses in the PM6:Y6 blend film upon illumination with AM 1.5 light filtered with a 400 nm long-pass filter were reduced by a factor of 1.4 and 1.8 for the PM6 and Y6 components, respectively. It is well established that high-energy UV photons can induce photodegradation of conjugated molecules by cleaving the weakest bonds in the molecule.[50,51] Finally, the PM6:Y6 film was exposed to AM 1.5 illumination filtered through a 665 nm long-pass filter (LP665). Under these conditions, light absorption in the long-wavelength region is primarily attributed to Y6, with only a minor contribution from the PM6 absorption tail. In Table 1 and Fig. 2(c), it is shown that PM6 and Y6 degrade by 15% and 7%, respectively, after exposure to LP665 for 45 h. Compared to unfiltered light, the exposure of the PM6:Y6 blend to LP665 light decreases the absorbance losses by a factor of 1.8 for PM6 and 2.3 for Y6. Notably, the donor PM6 still undergoes approximately 15% degradation after exposure of the PM6:Y6 blend film to LP665

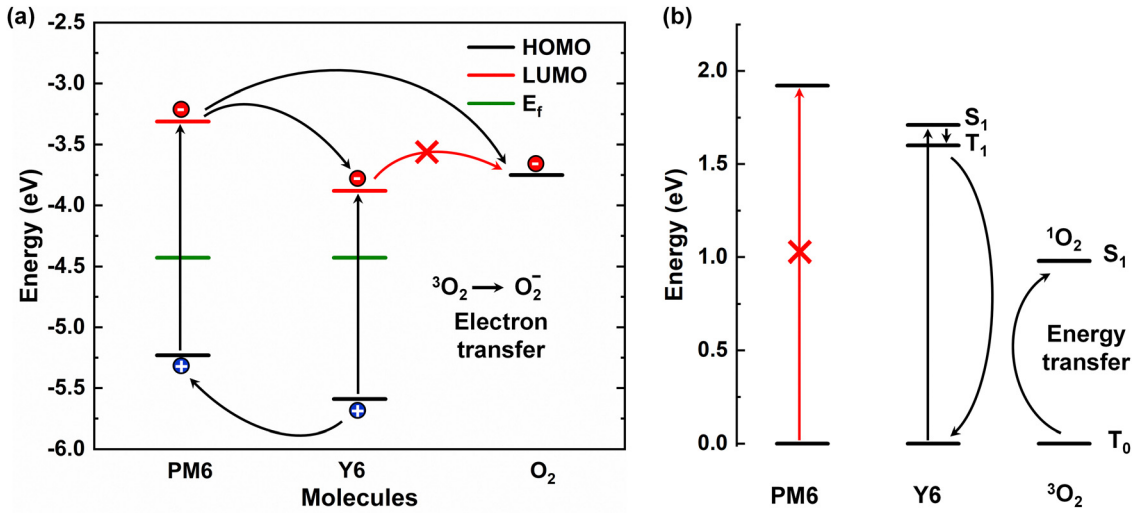

Fig. 3 (a) Energy level diagram of the PM6:Y6 blend, illustrating the allowed electron and hole transfer processes and O_2^- (superoxide) generation following the donor excitation under AM 1.5 light and LP400 conditions. The energy level diagram for PM6 and Y6, referenced to the vacuum level, was constructed using the work function and valence band onset values measured by UPS. For the optical band gap of PM6 and Y6, literature values were used.[52] (b) Energy level diagram of the PM6:Y6 blend, illustrating the energy transfer process from the acceptor to O_2, under LP665 illumination, resulting in $^1O_2$ (singlet oxygen) generation.

illumination for 45 h. Electron transfer from excited Y6 is prohibited under all illumination conditions, because the LUMO of the Y6 acceptor is lower (deeper) than the reduction potential of oxygen (Fig. 3(a)). Additionally, energy transfer from the excited state of Y6 to ground-state oxygen can occur, leading to the generation of singlet oxygen. This suggests that singlet oxygen is responsible for the degradation of both the acceptor and the donor under these illumination conditions, as illustrated in Fig. 3(b). To further investigate light-induced degradation, we quantified the absorbance losses of neat PM6, neat Y6, and a PM6:Y6 blend film after 45 h of LP665-filtered illumination. The neat PM6 and Y6 films exhibited absorbance decreases of 6% and 3%, respectively. In contrast, in the PM6:Y6 blend, the PM6 and Y6 components showed larger losses of 15% and 7%, respectively. These results indicate that both materials are less photostable in the blend than in their neat films and that PM6 degrades more rapidly than Y6 within the blend. The accelerated degradation observed in the blend is likely associated with energy transfer processes. Notably, the degradation of Y6 increases from 3% in the neat film to 7% in the blend under LP665-filtered light, indicating that the presence of the donor significantly accelerates the degradation rate, even under illumination conditions where the PM6 donor exhibits only minimal absorbance.

3.3 Analysis of photodegradation products

To investigate the photochemical degradation products upon exposure to light (AM 1.5), infrared spectra of films of PM6, Y6, and PM6 : Y6 (1 : 1), spin-coated on KBr substrates, were recorded in transmission mode. The samples were processed and photodegraded under the same conditions as those used for the UV-vis absorption spectroscopy.

Fig. 4 shows the FTIR spectra of PM6 (a), Y6 (b), and PM6:Y6 (c) films in the extended carbonyl region, ranging from 1850 cm^{-1} to 1570 cm^{-1}, before and after exposure to unfiltered white light (AM 1.5) in air for 45 h. The wide range FTIR spectra are shown in Fig. S4. The peak positions and their corresponding assignments are summarized in Tables S1 and S2. For PM6, the most significant changes after 45 h exposure are seen in the carbonyl region of the IR spectrum (Fig. 4(a)), namely the intensity drop of the sharp peak at 1649 cm^{-1}, corresponding to the C=O stretch in the quinone group, accompanied by the development of two new peaks with maxima at 1709 cm^{-1} and 1770 cm^{-1}.[53,54] The new peak at 1709 cm^{-1} can be assigned to the ester group, and the peak at 1770 cm^{-1} can be assigned to the anhydride group.[55] A similar growth of a peak at 1770 cm^{-1} has been observed in photo-oxidized PBDB-T and $PC_{60}BM$.[19,56,57] We also note that the peak at 1709 cm^{-1} grows 64% faster than the 1770 cm^{-1} peak. Smaller changes are also observed (see Fig. S4), such as a decrease in the absorption intensity of the four sharp peaks between 1400 and 1100 cm^{-1}, corresponding to C–H rocking and scissoring modes.[19,38,55,58] In addition, the peak intensities at ~1177 cm^{-1} and ~1550 cm^{-1} remain unchanged. The results indicate that PM6 undergoes photo-oxidation, affecting the quinone group, the side chains, and the backbone of the molecule. These findings contrast with the report by Wang *et al.*, indicating that photodegradation of PM6 under white-light exposure in air induces twisting of the BDT-T unit.[38]

Fig. 4(b) shows the carbonyl region of the IR spectra of Y6, characterized by two strong peaks, one at 1697 cm^{-1} that corresponds to the symmetric C=O stretch vibration of the terminal groups from the five-membered carbon ring and the other at 1600 cm^{-1}, which corresponds to the C=N stretch of the fused benzothiadiazole aromatic core.[53,55,59] In Fig. S4, we also identify the corresponding peaks for C≡N stretch vibration at 2216 cm^{-1} and 1535 cm^{-1} as malononitrile moieties dominated by C–C mode,[60] while the C=C stretch mode of thiophene is found at 1506 cm^{-1} and from the conjugate plane at 1426 cm^{-1}.[55] Upon photooxidation for 45 h, the Y6 films showed a minor decrease in the intensity of the peaks at 1535 cm^{-1}, 1426 cm^{-1}, 1290 cm^{-1}, 1253 cm^{-1}, 1230 cm^{-1}, and 1150 cm^{-1}. This indicates that the Y6 acceptor is less susceptible to degradation than the PM6 donor, in agreement with the UV-vis absorption spectra. The FTIR spectra of PM6 : Y6 (1 : 1) are shown in Fig. 4(c). The peak at 1649 cm^{-1} that was identified above as the C=O stretch in PM6 decreases rapidly upon photodegradation, as it did for neat PM6 films. New shoulders appear at 1722 cm^{-1} and 1770 cm^{-1} after exposure for 45 h, possibly indicating the formation of an ester and anhydride group. The peak at 1697 cm^{-1}, which was assigned to the C=O stretch, and the peak at 1600 cm^{-1} assigned to the C=N stretch of Y6 remain almost unchanged. The strong peaks

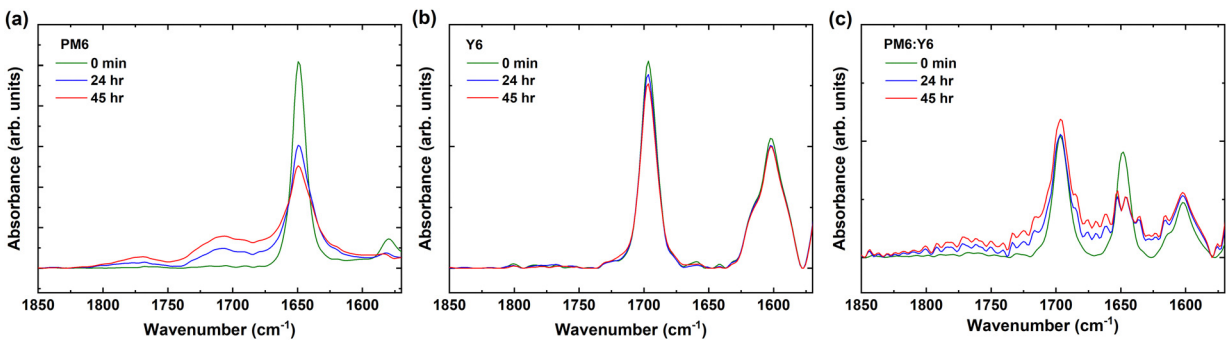

Fig. 4 FTIR spectra measured in transmission mode of spin-coated films of pristine (a) PM6, (b) Y6, and (c) PM6 : Y6 (1 : 1) on KBr, unexposed and exposed under white light (AM 1.5) for 45 h. The wide range spectra are shown in Fig. S4.

originating from Y6 at 2216 cm^{-1}, 1535 cm^{-1}, 1426 cm^{-1}, and 1290 cm^{-1} decrease, indicating that C≡N, malononitrile moieties, and C=C are also affected (see Fig. S4). The peaks at 1230 cm^{-1} and 1254 cm^{-1} show a smaller decrease in intensity compared to pure Y6 films. Interestingly, the intensities of the peaks at 1506 cm^{-1} and 1100 cm^{-1} remain unchanged, which was not the case for pure Y6 films. The peak positions of PM6:Y6 films can be compared with those in the IR spectra of the pure PM6 and Y6 films in Fig. S4. To further investigate the effect of light-induced degradation, the IR spectra of PM6:Y6 blend films exposed to LP400 and LP665 filtered light were measured and compared to the IR spectra of samples exposed to AM1.5 light, as shown in Fig. S5(a)–(c). As expected from the UV-vis absorption spectra, using the 400 nm and 665 nm long pass filter, the peak intensities of the strong IR peaks at 1149 cm^{-1}, 1230 cm^{-1}, 1290 cm^{-1}, 1426 cm^{-1}, and 1535 cm^{-1} were suppressed after 45 h of photodegradation (see Fig. S6). The emergence of new shoulder peaks at 1722 cm^{-1} and 1770 cm^{-1} after 45 h of exposure indicates the formation of ester and anhydride groups under both LP400 and LP665 filtered light, which were also suppressed. The peak at 1649 cm^{-1} is further suppressed under the LP665 condition compared to the no filter condition.

The AFM height images of pure PM6, pure Y6, and PM6:Y6 blend at 0 min and 45 h of exposure under simulated sunlight and ambient conditions are shown in Fig. S7. The height image of the 0 min PM6 and PM6:Y6 surface shows a fiber-like structure with surface roughness values of 0.98 nm and 0.77 nm, respectively. However, the Y6 films exhibit interconnected domains with a surface roughness of 1.27 nm. Upon exposure to light for 45 h under ambient conditions, the PM6, Y6, and PM6:Y6 films show a minor decrease in roughness with 0.96 nm, 1.24 nm, and 0.71 nm. From the AFM images, it can be concluded that after 45 h of photodegradation, the surface morphology of the pure PM6, pure Y6, and blend PM6:Y6 films remains unchanged.

To investigate the effects of photodegradation on the surfaces of PM6, Y6, and PM6:Y6 blend films, high-resolution XPS core-level spectra (C 1s, S 2p, O 1s, F 1s, and N 1s) and wide survey spectra were collected for both fresh (0 h) and photodegraded (45 h) samples. The survey spectrum of PM6, Y6, and PM6:Y6 is shown in Fig. S8.

Fig. 5 shows the core-level spectra of C 1s for the fresh (0 h) and degraded (45 h) samples of PM6, Y6, and PM6:Y6 blend films. In the C 1s spectra of PM6 at 0 h, presented in Fig. 5(a), the main peak at 285.17 eV corresponds to the C–C and C=C bonds of the aromatic rings and alkyl side chains, and the peak at 285.26 eV contains contributions from C–S and C–F bonds, while the 287.10 eV component represents the carbonyl of the quinone group. After 45 h of exposure to AM 1.5 light (Fig. 5(b)), the intensity of the main component at 285.17 eV decreases (see Fig. S9a), and a new peak appears at a higher binding energy of 289.61 eV. The peak at 285.26 eV, corresponding to C–S and C–F groups, grows and shifts towards higher binding energy at 285.54 eV. A decrease in the intensity of the main peak at 285.17 eV is observed, accompanied by a shift to a higher binding energy at 285.54 eV. The new peak at the higher binding energy of 289.61 eV is assigned to oxidized carbon after photooxidation. The FTIR spectra of PM6 support the formation of new carbonyls. Fig. 5(c) shows the C 1s spectra of Y6 for the fresh sample (0 h). The main peak at 284.82 eV is

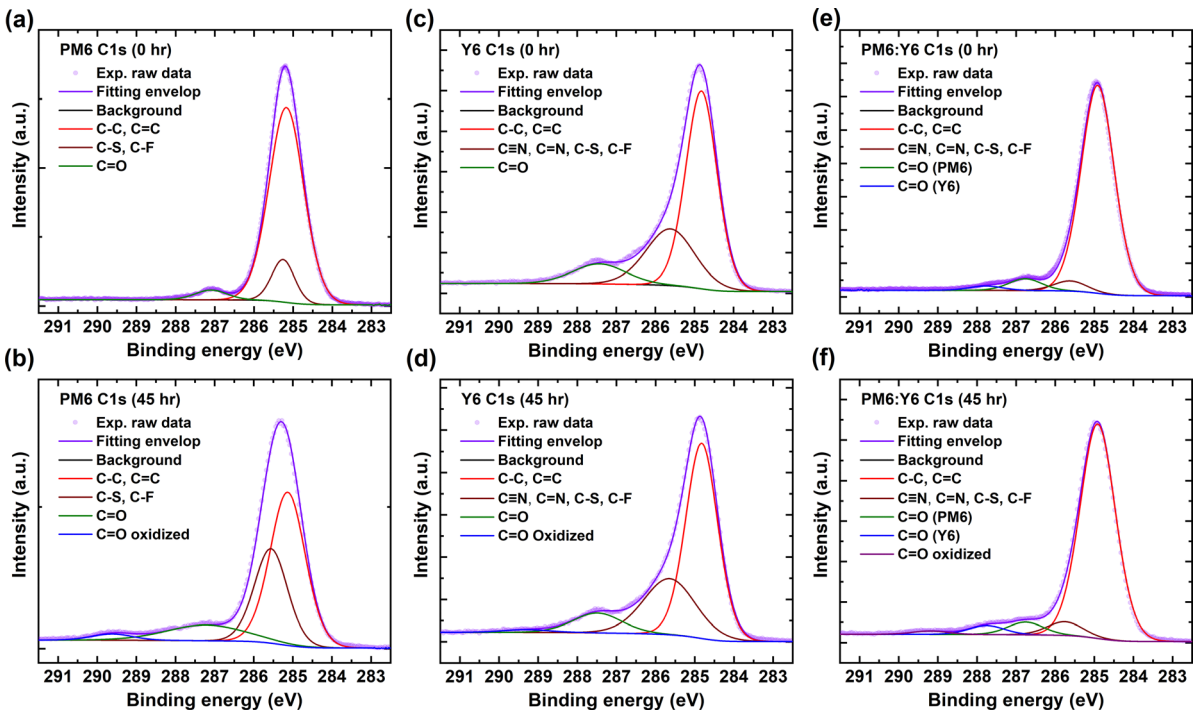

Fig. 5 High-resolution XPS core level C 1s spectra of (a, b) PM6, (c, d) Y6, and (e, f) PM6:Y6 blend films. Spectra are presented for fresh samples (0 h) and after 45 h of degradation under AM 1.5 illumination in air, as indicated in the legends.

assigned to C–C and C=C, originating from the aromatic rings and alkyl side chains. The peak at 285.62 eV corresponds to contributions from C–S, C–F, C=N, and C≡N groups, and the 287.43 eV component corresponds to the carbonyl from the terminal groups. The main peak at 284.82 eV decreases more slowly upon photodegradation compared to PM6 (see Fig. S9d), and a small new contribution starts to appear at 289.30 eV, as shown in Fig. 5(d), indicating the formation of new carbonyl groups upon photooxidation. The component at 285.62 eV, corresponding to the mixture of C–S, C–F, C=N, and C≡N bonds, shows an insignificant shift to 285.65 eV. Similarly, the peak at 287.43 eV, attributed to the carbonyl group, shifts insignificantly to 287.49 eV. The core-level C 1s spectra indicate that the Y6 acceptor is relatively more stable than PM6, which is consistent with the observations from the UV-vis and FTIR spectra following photooxidation. Fig. 5(e) shows the C 1s spectra of the PM6:Y6 blend film. The main peak at 284.92 eV corresponds to C–C and C=C bonds of both molecules, as observed in the pristine films. The peak at 285.62 eV corresponds to the mixture of peaks from C–S, C–F, C=N, and C≡N bonds. As expected, in the PM6:Y6 blend, the components at 286.77 eV and 287.77 eV correspond to the carbonyl groups from PM6 and Y6, respectively. After 45 h of exposure to AM 1.5 light (Fig. 5(f)), the main peak at 284.92 eV decreases (see Fig. S9g), while a new peak emerges at a higher binding energy of 289.20 eV. The carbonyl peaks from both the PM6 and Y6 show a minor shift to higher binding energies at 286.77 eV and 287.77 eV, respectively, upon photooxidation. The O 1s spectra of the PM6, Y6, and PM6:Y6 are shown in Fig. S9(c), (f) and (i). The increase in O 1s peak intensity confirms the addition of oxygen upon photooxidation. Moreover, the addition of oxygen is more pronounced in the PM6 samples compared to Y6 and the PM6:Y6 blend. The S 2p core level spectra of the PM6, Y6, and PM6:Y6 are shown in Fig. S10. After 45 h of degradation, new peaks appear at higher binding energies, indicating the formation of oxidized sulfur species (SO_x). For completeness, the F 1s core level spectra of PM6, Y6, and the PM6:Y6 blend at 0 h and after 45 h of photooxidation are shown in Fig. S11(a), (b) and (d). After 45 h of exposure, the F 1s spectra of PM6 exhibit only minor changes, indicating that the F 1s is only slightly affected upon photodegradation. Moreover, the F 1s spectra of both the Y6 acceptor and the PM6:Y6 blend remain essentially unchanged. Neither the N 1s core level spectra of Y6 nor the ones of PM6:Y6 blend show any significant changes after photooxidation, as presented in Fig. S11(c) and (e). These results suggest that the F 1s and N 1s core levels remain unaffected by the photodegradation process.

The effect on the frontier energy levels and the work function, induced by photodegradation of PM6, Y6, and the PM6:Y6 blend films, is investigated by the valence band (VB) and SECO spectra shown in Fig. 6. Fig. 6(a) shows the VB spectrum of a fresh and degraded (45 h) PM6 film. The valence band onset for the fresh PM6 film is estimated at 0.80 eV with respect to the Fermi level, E_F. After 45 h of degradation, the valence band decreases to 0.78 eV with respect to the Fermi level, and the valence band onset is difficult to determine from the UPS

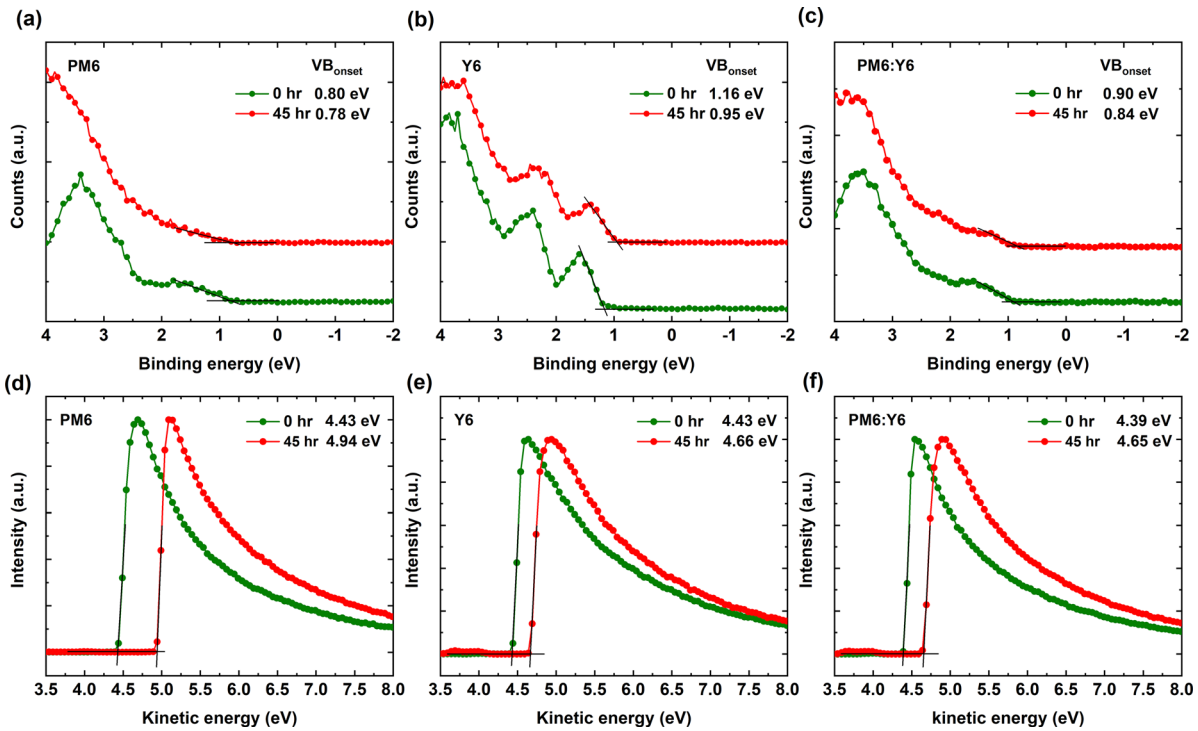

Fig. 6 Valence band spectra of (a) PM6, (b) Y6, and (c) PM6:Y6 blend films, along with the secondary electron cutoff (SECO) spectra of (d) PM6, (e) Y6, and (f) PM6:Y6. All spectra are shown for fresh samples (0 h) and after 45 h of degradation under AM 1.5 illumination in air. VB spectra of degraded films are intentionally offset on the *y*-axis for clarity. The VB onset and work function values are given in the VB spectra and SECO spectra, respectively.

spectrum. Also, the valence band spectra of Y6 (Fig. 6(b)) show a valence band onset decrease from 1.16 eV to 0.95 eV with respect to E_F upon 45 h of photodegradation. It is noteworthy that the shape of the density of states (DOS) for Y6 remains unchanged.

For the PM6:Y6 blend, the initial valence band onset of 0.90 eV decreases slightly to 0.84 eV following 45 h of degradation. The DOS of the blend is dominated by contributions from PM6.[21,61] From the secondary electron cutoff (SECO) spectra, shown in Fig. 6(d)–(f), the work function values of PM6, Y6, and the PM6:Y6 blend films were determined for fresh (0 h) and degraded (45 h) samples. Upon photodegradation, the work function of PM6 increases by 0.51 eV from 4.43 eV to 4.94 eV, while that of Y6 increases by 0.23 eV, from 4.43 eV to 4.66 eV. Similarly, the PM6:Y6 blend exhibits a work function increase of 0.26 eV from 4.39 eV to 4.65 eV. The increase in the work functions of PM6, Y6, and PM6:Y6 films can be related to chemical modifications upon photodegradation.[21] These results conclude that photodegradation induces distinct modifications in the frontier electronic structure across the donor, acceptor, and their blend.

4. Conclusions

We have studied the photodegradation of donor polymer PM6 and the small molecule acceptor Y6 and their blend PM6:Y6 in air under different illumination conditions. The UV-vis absorption spectra show that PM6 films photobleach significantly faster than Y6 films when exposed to AM1.5 light. Notably, the photodegradation of Y6 is accelerated in PM6:Y6 blend films compared to neat Y6 films. To differentiate the degradation pathways associated with reactive oxygen species, the PM6:Y6 blend film was additionally exposed to UV-filtered AM 1.5 light (LP400) and long-wavelength illumination (LP665). Exposure to filtered light results in slower degradation of the blend components compared to unfiltered light. When the blends are exposed to long-wavelength light (LP665), electron transfer is suppressed, thereby preventing the formation of superoxide radicals. The IR spectra of pure PM6 and PM6:Y6 blend films show the formation of new oxidized carbonyl groups and the breaking of the original quinone group upon photodegradation. Moreover, the C 1s and S 2p XPS spectra confirm the formation of the oxidized carbonyl groups and additionally oxidized sulfur at the surface of PM6, Y6, and PM6:Y6 films. After 45 h of photodegradation, shifts of 0.02 eV, 0.21 eV, and 0.06 eV on the valence band onset towards the Fermi level for PM6, Y6, and PM6:Y6 samples after exposure are observed. The work function increases after degradation, which could indicate chemical modifications across all samples. This work could inspire the design of new donor and acceptor materials by tuning their singlet and triplet states to prevent photodegradation caused by oxygen-mediated species.

Author contributions

SP prepared all the samples; conducted the degradation experiments; measured the UV-vis absorption spectra, FTIR spectra, and AFM images; and drafted the first version of the manuscript. SP and EM conducted XPS, VB, and SECO measurements with the help of other co-workers. EM and MA supervised the work, contributed to the data analysis and interpretation of the results, and assisted in writing the manuscript. All authors contributed to the final version of the manuscript.

Conflicts of interest

The authors have no conflicts of interest.

Data availability

The data supporting this article have been included as part of the supplementary information (SI). Supplementary information is available. See DOI: https://doi.org/10.1039/d5tc03779d.

Acknowledgements

The authors would like to thank Dr Hanmin Zhang, Dr Cleber F. N. Marchiori, Dr Leif K. E. Ericsson, Dr Saurabh Pareek, and Shahna Mysin Kadakkotteeri for their help with XPS and UPS measurements at the MAX IV synchrotron. The authors would also like to thank the beamline scientists, Dr Alexei Preobrajenski, Dr Alexander Generalov, and Dr Stephan Appelfeller, for their assistance with the synchrotron measurements. We acknowledge the MAX IV Laboratory for beamtime on the FlexPES beamline under proposal 20241616. Research conducted at MAX IV, a Swedish national user facility, is supported by Vetenskapsrådet (Swedish Research Council, VR) under contract 2018-07152. We acknowledge funding through the PRISMAS program from the European Union's COFUND action, within the European Commission MSCA framework (grant agreement ID: 101081419). EM acknowledges the Swedish Energy Agency for financial support of the project (contract 48598-1) and for the funding of the colla. The (grant number 2016.0059) is acknowledged for financial support for the research equipment used in the project.

References

1 Y. Li, G. Xu, C. Cui and Y. Li, Flexible and Semitransparent Organic Solar Cells, *Adv. Energy Mater.*, 2018, **8**, 1701791.
2 L. Sun, K. Fukuda and T. Someya, Recent progress in solution-processed flexible organic photovoltaics, *npj Flexible Electron.*, 2022, **6**, 89.
3 F. Yang, Y. Huang, Y. Li and Y. Li, Large-area flexible organic solar cells, *npj Flexible Electron.*, 2021, **5**, 30.
4 R. García-Valverde, J. A. Cherni and A. Urbina, Life cycle analysis of organic photovoltaic technologies, *Prog. Photovoltaics Res. Appl.*, 2010, **18**, 535–558.
5 S. Lizin, S. Van Passel, E. De Schepper, W. Maes, L. Lutsen, J. Manca and D. Vanderzande, Life cycle analyses of organic photovoltaics: a review, *Energy Environ. Sci.*, 2013, **6**, 3136–3149.
6 D. Yue, P. Khatav, F. You and S. B. Darling, Deciphering the uncertainties in life cycle energy and environmental

analysis of organic photovoltaics, *Energy Environ. Sci.*, 2012, **5**, 9163–9172.
7 D. Luo, W. Jang, D. D. Babu, M. S. Kim, D. H. Wang and A. K. K. Kyaw, Recent progress in organic solar cells based on non-fullerene acceptors: materials to devices, *J. Mater. Chem. A*, 2022, **10**, 3255–3295.
8 N. Ahmad, J. Yuan and Y. Zou, One more step towards better stability of non-fullerene organic solar cells: advances, challenges, future perspectives, and the Era of artificial intelligence, *Energy Environ. Sci.*, 2025, **18**, 5093–5158.
9 Y. Zhang, W. Deng, C. E. Petoukhoff, X. Xia, Y. Lang, H. Xia, H. Tang, H. T. Chandran, S. Mahadevan, K. Liu, P. W. K. Fong, Y. Luo, J. Wu, S.-W. Tsang, F. Laquai, H. Wu, X. Lu, Y. Yang and G. Li, Achieving 19.4% organic solar cell *via* an *in situ* formation of p–i–n structure with built-in interpenetrating network, *Joule*, 2024, **8**, 509–526.
10 D. Meng, R. Zheng, Y. Zhao, E. Zhang, L. Dou and Y. Yang, Near-Infrared Materials: The Turning Point of Organic Photovoltaics, *Adv. Mater.*, 2022, **34**, 2107330.
11 Z. Ling, J. Wu, J. P. Jurado, C. E. Petoukhoff, S. Y. Jeong, D. Naphade, M. Babics, X. Chang, H. Faber, S. Doukas, E. Lidorikis, M. I. Nugraha, M. He, M. Alqurashi, Y. Lin, X. Sun, H. Hu, H. Y. Woo, S. De Wolf, L. Tsetseris, F. Laquai, D. Yu, E. Wang and T. D. Anthopoulos, 20.5% efficient ternary organic photovoltaics using an asymmetric small-molecular acceptor to manipulate intermolecular packing and reduce energy losses, *Mater. Sci. Eng., R*, 2025, **163**, 100922.
12 J. Han, H. Xu, S. H. K. Paleti, A. Sharma and D. Baran, Understanding photochemical degradation mechanisms in photoactive layer materials for organic solar cells, *Chem. Soc. Rev.*, 2024, **53**, 7426–7454.
13 M. Riede, D. Spoltore and K. Leo, Organic Solar Cells—The Path to Commercial Success, *Adv. Energy Mater.*, 2021, **11**, 2002653.
14 B. Azzopardi, C. J. M. Emmott, A. Urbina, F. C. Krebs, J. Mutale and J. Nelson, Economic assessment of solar electricity production from organic-based photovoltaic modules in a domestic environment, *Energy Environ. Sci.*, 2011, **4**, 3741–3753.
15 L. Duan and A. Uddin, Progress in Stability of Organic Solar Cells, *Adv. Sci.*, 2020, **7**, 1903259.
16 Y. Li, T. Li and Y. Lin, Stability: next focus in organic solar cells based on non-fullerene acceptors, *Mater. Chem. Front.*, 2021, **5**, 2907–2930.
17 P. Cheng and X. Zhan, Stability of organic solar cells: challenges and strategies, *Chem. Soc. Rev.*, 2016, **45**, 2544–2582.
18 P. Weitz, J. Wortmann, C. Liu, T.-J. Wen, C.-Z. Li, T. Heumüller and C. J. Brabec, Photodegradation of Organic Solar Cells under Visible Light and the Crucial Influence of Its Spectral Composition, *ACS Appl. Mater. Interfaces*, 2024, **16**, 36667–36677.
19 S. Prasad, Z. Genene, C. F. N. Marchiori, S. Singh, L. K. E. Ericsson, E. Wang, C. M. Araujo and E. Moons, Effect of molecular structure on the photochemical stability of acceptor and donor polymers used in organic solar cells, *Mater. Adv.*, 2024, **5**, 7708–7720.
20 M. Hermenau, M. Riede, K. Leo, S. A. Gevorgyan, F. C. Krebs and K. Norrman, Water and oxygen induced degradation of small molecule organic solar cells, *Sol. Energy Mater. Sol. Cells*, 2011, **95**, 1268–1277.
21 Q. Zhang, Y. Chen, X. Liu and M. Fahlman, *In situ* near-ambient pressure X-ray photoelectron spectroscopy reveals the effects of water, oxygen and light on the stability of PM6:Y6 photoactive layers, *J. Mater. Chem. C*, 2023, **11**, 3112–3118.
22 Z.-X. Liu, Z.-P. Yu, Z. Shen, C. He, T.-K. Lau, Z. Chen, H. Zhu, X. Lu, Z. Xie, H. Chen and C.-Z. Li, Molecular insights of exceptionally photostable electron acceptors for organic photovoltaics, *Nat. Commun.*, 2021, **12**, 3049.
23 A. J. Clarke, J. Luke, R. Meitzner, J. Wu, Y. Wang, H. K. H. Lee, E. M. Speller, H. Bristow, H. Cha, M. J. Newman, K. Hooper, A. Evans, F. Gao, H. Hoppe, I. McCulloch, U. S. Schubert, T. M. Watson, J. R. Durrant, W. C. Tsoi, J.-S. Kim and Z. Li, Non-fullerene acceptor photostability and its impact on organic solar cell lifetime, *Cell Rep. Phys. Sci.*, 2021, **2**, 100498.
24 P. Jiang, L. Hu, L. Sun, Z. A. Li, H. Han and Y. Zhou, On the interface reactions and stability of nonfullerene organic solar cells, *Chem. Sci.*, 2022, **13**, 4714–4739.
25 Y. Jiang, L. Sun, F. Jiang, C. Xie, L. Hu, X. Dong, F. Qin, T. Liu, L. Hu, X. Jiang and Y. Zhou, Photocatalytic effect of ZnO on the stability of nonfullerene acceptors and its mitigation by SnO_2 for nonfullerene organic solar cells, *Mater. Horiz.*, 2019, **6**, 1438–1443.
26 H. Zhao, N. Prine, S. Kundu, G. Ma and X. Gu, Effect of Thermal Stress on Morphology in High-Performance Organic Photovoltaic Blends, *JACS Au*, 2024, **4**, 4334–4344.
27 A. Rivaton, A. Tournebize, J. Gaume, P.-O. Bussière, J.-L. Gardette and S. Therias, Photostability of organic materials used in polymer solar cells, *Polym. Int.*, 2014, **63**, 1335–1345.
28 M. Jørgensen, K. Norrman and F. C. Krebs, Stability/degradation of polymer solar cells, *Sol. Energy Mater. Sol. Cells*, 2008, **92**, 686–714.
29 E. M. Speller, A. J. Clarke, N. Aristidou, M. F. Wyatt, L. Francàs, G. Fish, H. Cha, H. K. H. Lee, J. Luke, A. Wadsworth, A. D. Evans, I. McCulloch, J.-S. Kim, S. A. Haque, J. R. Durrant, S. D. Dimitrov, W. C. Tsoi and Z. Li, Toward Improved Environmental Stability of Polymer:Fullerene and Polymer:-Nonfullerene Organic Solar Cells: A Common Energetic Origin of Light- and Oxygen-Induced Degradation, *ACS Energy Lett.*, 2019, **4**, 846–852.
30 E. T. Hoke, I. T. Sachs-Quintana, M. T. Lloyd, I. Kauvar, W. R. Mateker, A. M. Nardes, C. H. Peters, N. Kopidakis and M. D. McGehee, The Role of Electron Affinity in Determining Whether Fullerenes Catalyze or Inhibit Photooxidation of Polymers for Solar Cells, *Adv. Energy Mater.*, 2012, **2**, 1351–1357.
31 Y. Li, K.-K. Liu, F. R. Lin and A. K.-Y. Jen, Improving the Stability of Organic Solar Cells: From Materials to Devices, *Sol. RRL*, 2023, **7**, 2300531.
32 A. Tournebize, A. Rivaton, H. Peisert and T. Chassé, The Crucial Role of Confined Residual Additives on the Photostability of P3HT:PCBM Active Layers, *J. Phys. Chem. C*, 2015, **119**, 9142–9148.

33 M. Qin, P. Cheng, J. Mai, T.-K. Lau, Q. Zhang, J. Wang, C. Yan, K. Liu, C.-J. Su, W. You, X. Lu and X. Zhan, Enhancing Efficiency and Stability of Organic Solar Cells by UV Absorbent, *Sol. RRL*, 2017, **1**, 1700148.

34 V. Turkovic, S. Engmann, N. Tsierkezos, H. Hoppe, M. Madsen, H.-G. Rubahn, U. Ritter and G. Gobsch, Long-term stabilization of organic solar cells using UV absorbers, *J. Phys. D: Appl. Phys.*, 2016, **49**, 125604.

35 Y. Cui, Z. Chen, P. Zhu, W. Ma, H. Zhu, X. Liao and Y. Chen, Enhancing photostability and power conversion efficiency of organic solar cells by a ''sunscreen'' ternary strategy, *Sci. China: Chem.*, 2023, **66**, 1179–1189.

36 N. Gasparini, M. Salvador, S. Strohm, T. Heumueller, I. Levchuk, A. Wadsworth, J. H. Bannock, J. C. de Mello, H.-J. Egelhaaf, D. Baran, I. McCulloch and C. J. Brabec, Burn-in Free Nonfullerene-Based Organic Solar Cells, *Adv. Energy Mater.*, 2017, **7**, 1700770.

37 H. Cha, J. Wu, A. Wadsworth, J. Nagitta, S. Limbu, S. Pont, Z. Li, J. Searle, M. F. Wyatt, D. Baran, J.-S. Kim, I. McCulloch and J. R. Durrant, An Efficient, ''Burn in'' Free Organic Solar Cell Employing a Nonfullerene Electron Acceptor, *Adv. Mater.*, 2017, **29**, 1701156.

38 Y. Wang, J. Luke, A. Privitera, N. Rolland, C. Labanti, G. Londi, V. Lemaur, D. T. W. Toolan, A. J. Sneyd, S. Jeong, D. Qian, Y. Olivier, L. Sorace, J.-S. Kim, D. Beljonne, Z. Li and A. J. Gillett, The critical role of the donor polymer in the stability of high-performance non-fullerene acceptor organic solar cells, *Joule*, 2023, **7**, 810–829.

39 I. V. Martynov, L. N. Inasaridze and P. A. Troshin, Resist or Oxidize: Identifying Molecular Structure–Photostability Relationships for Conjugated Polymers Used in Organic Solar Cells, *ChemSusChem*, 2022, **15**, e202101336.

40 T. Liu, Q. C. Burlingame, M. R. Ivancevic, X. Liu, J. Hu, B. P. Rand and Y.-L. Loo, Photochemical Decomposition of Y-Series Non-Fullerene Acceptors Is Responsible for Degradation of High-Efficiency Organic Solar Cells, *Adv. Energy Mater.*, 2023, **13**, 2300046.

41 A. Preobrajenski, A. Generalov, G. Ohrwall, M. Tchaplyguine, H. Tarawneh, S. Appelfeller, E. Frampton and N. Walsh, FlexPES: a versatile soft X-ray beamline at MAX IV Laboratory, *J. Synchrotron Radiat.*, 2023, **30**, 831–840.

42 N. Fairley, V. Fernandez, M. Richard-Plouet, C. Guillot-Deudon, J. Walton, E. Smith, D. Flahaut, M. Greiner, M. Biesinger, S. Tougaard, D. Morgan and J. Baltrusaitis, Systematic and collaborative approach to problem solving using X-ray photoelectron spectroscopy, *Appl. Surf. Sci. Adv.*, 2021, **5**, 100112.

43 J. H. Scofield, Hartree-Slater subshell photoionization cross-sections at 1254 and 1487 eV, *J. Electron Spectrosc. Relat. Phenom.*, 1976, **8**, 129–137.

44 A. Proctor and P. M. A. Sherwood, Data analysis techniques in x-ray photoelectron spectroscopy, *Anal. Chem.*, 1982, **54**, 13–19.

45 S. Hüfner, in *Photoelectron Spectroscopy: Principles and Applications* ed. S. Hüfner, Springer, Berlin Heidelberg, 2003, pp. 1–60.

46 P. Urbánek, I. Kuřitka, J. Ševčík, J. Toušková, J. Toušek, V. Nádaždy, P. Nádaždy, K. Végsö, P. Šiffalovič, R. Rutsch and M. Urbánek, An experimental and theoretical study of the structural ordering of the PTB7 polymer at a mesoscopic scale, *Polymer*, 2019, **169**, 243–254.

47 Y. Liu, K. Zhou, X. Zhou, W. Xue, Z. Bi, H. Wu, Z. Ma and W. Ma, Strengthening the Intermolecular Interaction of Prototypical Semicrystalline Conjugated Polymer Enables Improved Photocurrent Generation at the Heterojunction, *Macromol. Rapid Commun.*, 2022, **43**, 2100871.

48 Y. W. Soon, H. Cho, J. Low, H. Bronstein, I. McCulloch and J. R. Durrant, Correlating triplet yield, singlet oxygen generation and photochemical stability in polymer/fullerene blend films, *Chem. Commun.*, 2013, **49**, 1291–1293.

49 M. Manceau, E. Bundgaard, J. E. Carlé, O. Hagemann, M. Helgesen, R. Søndergaard, M. Jørgensen and F. C. Krebs, Photochemical stability of π-conjugated polymers for polymer solar cells: a rule of thumb, *J. Mater. Chem.*, 2011, **21**, 4132–4141.

50 J. B. Patel, P. Tiwana, N. Seidler, G. E. Morse, O. R. Lozman, M. B. Johnston and L. M. Herz, Effect of Ultraviolet Radiation on Organic Photovoltaic Materials and Devices, *ACS Appl. Mater. Interfaces*, 2019, **11**, 21543–21551.

51 A. Classen, T. Heumueller, I. Wabra, J. Gerner, Y. He, L. Einsiedler, N. Li, G. J. Matt, A. Osvet, X. Du, A. Hirsch and C. J. Brabec, Revealing Hidden UV Instabilities in Organic Solar Cells by Correlating Device and Material Stability, *Adv. Energy Mater.*, 2019, **9**, 1902124.

52 J. Bertrandie, J. Han, C. S. P. De Castro, E. Yengel, J. Gorenflot, T. Anthopoulos, F. Laquai, A. Sharma and D. Baran, The Energy Level Conundrum of Organic Semiconductors in Solar Cells, *Adv. Mater.*, 2022, **34**, 2202575.

53 T. Shan, Y. Zhang, Y. Wang, Z. Xie, Q. Wei, J. Xu, M. Zhang, C. Wang, Q. Bao, X. Wang, C.-C. Chen, J. Huang, Q. Chen, F. Liu, L. Chen and H. Zhong, Universal and versatile morphology engineering *via* hot fluorous solvent soaking for organic bulk heterojunction, *Nat. Commun.*, 2020, **11**, 5585.

54 S. H. K. Paleti, S. Hultmark, J. Han, Y. Wen, H. Xu, S. Chen, E. Järsvall, I. Jalan, D. R. Villalva, A. Sharma, J. I. Khan, E. Moons, R. Li, L. Yu, J. Gorenflot, F. Laquai, C. Müller and D. Baran, Hexanary blends: a strategy towards thermally stable organic photovoltaics, *Nat. Commun.*, 2023, **14**, 4608.

55 J. Coates, Interpretation of infrared spectra, a practical approach, *Encyclopedia of analytical chemistry*, 2000, vol. 12, pp. 10815–10837.

56 I. E. Brumboiu, L. K. E. Ericsson, V. Blazinic, R. Hansson, A. Opitz, B. Brena and E. Moons, Photooxidation of PC60BM: new insights from spectroscopy, *Phys. Chem. Chem. Phys.*, 2022, **24**, 25753–25766.

57 S. Chambon, A. Rivaton, J.-L. Gardette and M. Firon, Photo- and thermal degradation of MDMO-PPV:PCBM blends, *Sol. Energy Mater. Sol. Cells*, 2007, **91**, 394–398.

58 J. Guo, Y. Wu, R. Sun, W. Wang, J. Guo, Q. Wu, X. Tang, C. Sun, Z. Luo, K. Chang, Z. Zhang, J. Yuan, T. Li, W. Tang, E. Zhou, Z. Xiao, L. Ding, Y. Zou, X. Zhan, C. Yang, Z. Li,

C. J. Brabec, Y. Li and J. Min, Suppressing photo-oxidation of non-fullerene acceptors and their blends in organic solar cells by exploring material design and employing friendly stabilizers, *J. Mater. Chem. A*, 2019, **7**, 25088–25101.

59 J. Zhang, J. Guan, Y. Zhang, S. Qin, Q. Zhu, X. Kong, Q. Ma, X. Li, L. Meng, Y. Yi, J. Zheng and Y. Li, Direct Observation of Increased Free Carrier Generation Owing to Reduced Exciton Binding Energies in Polymerized Small-Molecule Acceptors, *J. Phys. Chem. Lett.*, 2022, **13**, 8816–8824.

60 M. Nuber, L. V. Spanier, S. Roth, G. N. Vayssilov, R. Kienberger, P. Müller-Buschbaum and H. Iglev, Picosecond Charge-Transfer-State Dynamics in Wide Band Gap Polymer-Non-Fullerene Small-Molecule Blend Films Investigated *via* Transient Infrared Spectroscopy, *J. Phys. Chem. Lett.*, 2022, **13**, 10418–10423.

61 D. Neusser, B. Sun, W. L. Tan, L. Thomsen, T. Schultz, L. Perdigón-Toro, N. Koch, S. Shoaee, C. R. McNeill, D. Neher and S. Ludwigs, Spectroelectrochemically determined energy levels of PM6:Y6 blends and their relevance to solar cell performance, *J. Mater. Chem. C*, 2022, **10**, 11565–11578.

